HHS Public Access

Author manuscript

Cell Rep. Author manuscript; available in PMC 2023 July 11.

Published in final edited form as:

Cell Rep. 2023 May 30; 42(5): 112455. doi:10.1016/j.celrep.2023.112455.

A tug of war between DCC and ROBO1 signaling during commissural axon guidance

Brianna Dailey-Krempel[1,4], **Andrew L. Martin**[1,3,4], **Ha-Neul Jo**[2], **Harald J. Junge**[2], **Zhe Chen**[1,5,*]

[1]Department of Neuroscience, University of Minnesota, Minneapolis, MN 55455, USA

[2]Department of Ophthalmology and Visual Neurosciences, University of Minnesota, Minneapolis, MN 55455, USA

[3]Present address: Washington University in St. Louis, St. Louis, MO, USA

[4]These authors contributed equally

[5]Lead contact

SUMMARY

Dynamic and coordinated axonal responses to changing environments are critical for establishing neural connections. As commissural axons migrate across the CNS midline, they are suggested to switch from being attracted to being repelled in order to approach and to subsequently leave the midline. A molecular mechanism that is hypothesized to underlie this switch in axonal responses is the silencing of Netrin1/Deleted in Colorectal Carcinoma (DCC)-mediated attraction by the repulsive SLIT/ROBO1 signaling. Using *in vivo* approaches including CRISPR-Cas9-engineered mouse models of distinct *Dcc* splice isoforms, we show here that commissural axons maintain responsiveness to both Netrin and SLIT during midline crossing, although likely at quantitatively different levels. In addition, full-length DCC in collaboration with ROBO3 can antagonize ROBO1 repulsion *in vivo*. We propose that commissural axons integrate and balance the opposing DCC and Roundabout (ROBO) signaling to ensure proper guidance decisions during midline entry and exit.

Graphical Abstract

*Correspondence: chen6867@umn.edu.

AUTHOR CONTRIBUTIONS

Z.C. conceived and designed the study. B.D.K., A.L.M., H.N.J., and Z.C. conducted the experiments and analyzed the data. B.D.K., A.L.M., H.N.J., H.J.J., and Z.C. wrote the manuscript.

SUPPLEMENTAL INFORMATION

Supplemental information can be found online at https://doi.org/10.1016/j.celrep.2023.112455.

DECLARATION OF INTERESTS

The authors declare no competing interests.

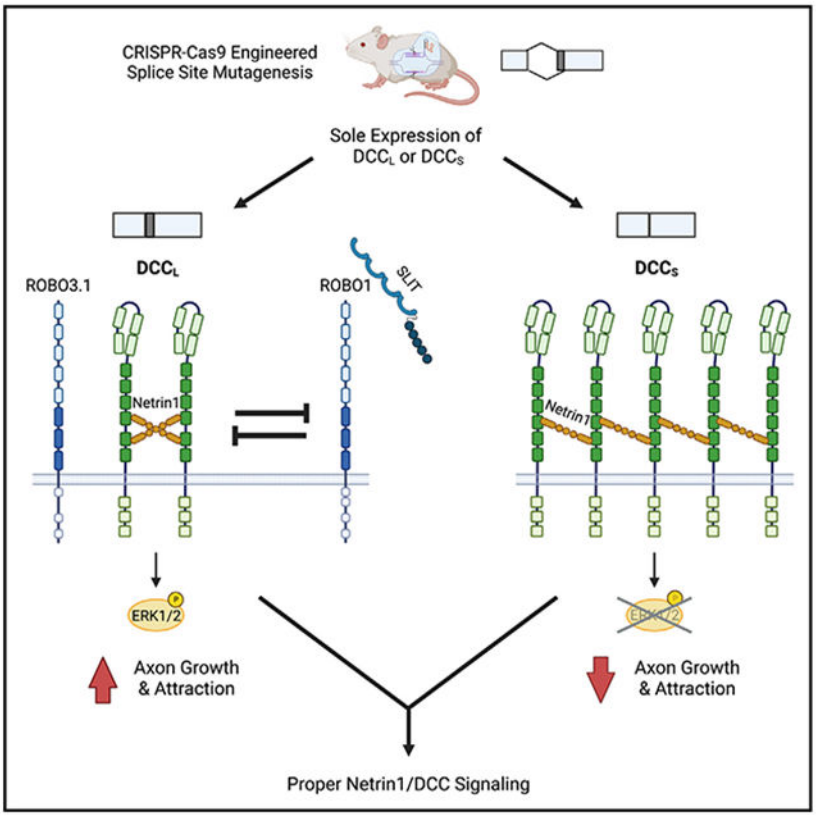

In brief

Using CRISPR-Cas9-engineered *Dcc* isoform mutants, Dailey-Krempel et al. show that Netrin1/DCC and SLIT/ROBO1 signaling are engaged in a counteraction akin to a tug of war in regulating axon guidance *in vivo*.

INTRODUCTION

Navigating axons encounter diverse environmental cues and thus need to dynamically regulate transmembrane receptors and downstream signaling pathways to elicit appropriate responses. Contralaterally projecting commissural axons connect the bilaterally organized CNS and are components of major neural circuits. In the mammalian spinal cord, a number of molecules are involved in directing the commissural axons toward and across the ventral midline, including prototypical attractive and repulsive molecules (e.g., Netrin1[1] and SLIT,[2] respectively), classical morphogens (e.g., bone morphogenetic proteins [BMPs][3,4] and sonic hedgehog [SHH][5]), growth factors (e.g., vascular endothelial growth factor [VEGF][6]), and others (e.g., neural EGFL-like2 [NELL2][7] and dorsal inhibitory axon guidance protein [Draxin][8]) (also see review[9]). How the axons incorporate the activities of the different receptors and downstream signaling cascades at temporal and spatial levels remains poorly understood.

Among the signaling pathways are the evolutionarily conserved Netrin1/Deleted in Colorectal Carcinoma (DCC) and SLIT/Roundabout (ROBO) ligand/receptor pairs, which

also have important functions beyond axon guidance and outside the nervous system.[10-13] While Netrin1/DCC promotes commissural axon growth and ventral projection toward the floorplate (FP), SLIT/ROBO elicits repulsion to facilitate axon exit from the midline and to block the axons from recrossing.[14,15] Previous studies using *in vitro* cultures have suggested binary and opposite responses to Netrin1 and SLIT in spinal commissural axons at the midline; i.e., the axons are attracted to Netrin1 and are nonresponsive to SLIT pre-crossing, but switch to being nonresponsive to Netrin1 and being repelled by SLIT post-crossing.[16-18] This "midline switch" would allow the axons to approach and subsequently leave the midline.[14,15]

At the receptor level, the molecular mechanisms that underlie the differential responses to Netrin1 and SLIT include (1) distinct receptor localizations in pre- and post-crossing axonal domains, (2) heterodimerization between DCC and ROBO1, and (3) modulation of DCC and ROBO1 activities by coreceptors. For example, several protein and microRNA factors contribute to the regulation of ROBO1 protein levels and surface localization in spinal commissural axons,[19-23] which are low in pre-crossing axonal segments and are significantly upregulated post crossing.[24] In addition, *in vitro* assays suggest that ROBO1, upon being upregulated at the midline and bound by SLIT2, directly bind and inactivate DCC.[25] Furthermore, ROBO3, specifically the ROBO3A.1/ROBO3.1 isoform that is expressed in pre-crossing axons,[26] functions as a coreceptor for DCC to potentiate Netrin1 attraction.[27] ROBO3.1 also inhibits ROBO1/2 repulsion through an unknown mechanism.[18,26]

While silencing of DCC by ROBO1 is proposed for spinal commissural axons, *in vitro* assays of callosal axons, the largest commissural populations in the brain, suggests the opposite (i.e., Netrin1/DCC repressing SLIT/ROBO1 repulsion).[28] Additional modes of DCC/ROBO1 interaction have also been suggested for other neuronal populations, including the two acting simultaneously and independently in spinal motor neurons/axons and pioneer longitudinal axons,[29-31] and SLIT/ROBO1 inducing Netrin1/DCC attraction in the presence of FLRT3 in thalamocortical axons.[32] Thus, the DCC/ROBO1 relationship is complex and remains to be further elucidated *in vivo*.

We have previously shown that two distinct DCC isoforms, i.e., full-length DCC_{long} and truncated DCC_{short}, with the latter missing 20 aa in the extracellular domain (referred to as DCC_L and DCC_S hereafter), are generated through developmentally regulated alternative splicing[33,34] (Figure 1A). Using genetic approaches, including CRISPR-Cas9-engineered mouse models, where either DCC isoform is solely expressed, we report here that Netrin1/DCC and SLIT/ROBO1 signaling are active simultaneously and antagonize each other throughout commissural axon midline crossing *in vivo*. Our data also show that, in order to achieve proper responses to Netrin1 around the midline, the presence of both DCC variants is required. While full-length DCC_L antagonizes ROBO1 repulsion to facilitate midline entry, its persistent expression blocks midline exit. By contrast, DCC_S, a truncated isoform that cannot activate Netrin1-induced signaling, reduces midline entry but is required to allow midline exit.

RESULTS

Two distinct *Dcc* isoforms are expressed during commissural axon guidance

In the spinal cord, both Dcc_L and Dcc_S are expressed over the period from commissural neurogenesis to the end of midline crossing (E11 to E15 in rats and E9.5 to E13.5 in mice), and their levels are comparable during the peak of crossing between E10.5 and E11.5 (Figures 1B and 1C).

Although both isoforms bind Netrin1 with high affinity, they adopt distinct conformations when in complex with Netrin1.[35] DCC_S forms a continuous ligand/receptor assembly with Netrin1, resulting in a high-molecular-weight complex. By contrast, DCC_L, which is modeled after the Neogenin homolog, is likely to adopt a 2:2 ligand:receptor heterotetramer.[35]

Using cultured COS-1 cells, we compared the isoforms in activating the ERK1/2 MAP kinases in response to Netrin1, which is important for commissural axon outgrowth.[36] We found that while DCC_L was able to induce a transient and strong activation of ERK1/2 phosphorylation upon Netrin1 stimulation, DCC_S did not exhibit this activity (Figures 1D and 1E). Thus, the isoforms have differential signaling abilities, likely as a result of the distinct structures.

Generation of CRISPR-Cas9-engineered mouse models where one of two *Dcc* splice isoforms is solely expressed

To determine the physiological role of *Dcc* isoforms, we generated mouse models where only one of the two is expressed. We designed guide RNAs (gRNAs) that can direct Cas9 endonuclease to the genomic sequences at or near the two alternative splice sites (Figures 2A and S1). We injected the gRNAs and Cas9 mRNA into pronuclei of mouse embryos and identified animals that harbored mutations in the desired regions by Sanger sequencing (Figure S1). We then cloned the mutated genomic sequences into a minigene *in vitro* splicing reporter,[33] expressed the reporter in cultured COS-1 cells, and determined the effect of the mutations on *Dcc* isoform production using RT-PCR and Sanger sequencing (Figure S1). Afterward, we selected the mutants that led to sole expression of either isoform, outbred them with the CD-1 strain for more than six generations, and characterized homozygous mice for axon guidance phenotypes (Figures 2B and 2C, also see details in STAR Methods). Hereafter, we refer to the mutants where either isoform is solely expressed as Dcc_L^{SE} and Dcc_S^{SE}, respectively.

For each isoform, two independent founder lines with different genomic mutations were characterized and were found to be phenotypically indistinguishable from each other. The two independent Dcc_L^{SE} mutations deleted 9 and 13 bp, respectively, upstream of the Dcc_L splice site (Figures 2B and S1B). These mutations enhanced the usage of the splice site and resulted in the sole expression of Dcc_L in homozygotes (Figure 2C). Similarly, an 11-bp deletion upstream of the Dcc_S splice site produced Dcc_S exclusively. A second Dcc_S^{SE} mutation deleted the Dcc_L splice site and the surrounding sequences and simultaneously introduced a 6-bp insertion (Figures 2B, 2C, S1B, and S1C).

Using quantitative RT-PCR and western blotting, we found that the overall levels of *Dcc* mRNA and protein in the isoform mutants were comparable with those in wild-type (WT) mice (Figure S2). Using immunostaining with specific antibodies, we also found that DCC was localized to both pre- and post-crossing axonal segments in the isoform mutants, similar to WT controls (Figure 2D). Thus, the isoforms are expressed by the same neurons/axons and have comparable spatial distribution.

Expressing Dcc_L alone increases commissural axon growth but blocks midline exit, whereas expressing Dcc_S alone reduces axon growth and delays midline entry

Using explants of dorsal spinal cord (DSC), which contain commissural interneuron somas, we examined axon outgrowth in response to Netrin1 in the isoform mutants. We found that in 3D collagen matrix and in the presence of bath-applied Netrin1, the amount of axons extending out of the explants was increased by 37% in Dcc_L^{SE} mutants compared with WT controls but was decreased by 32% in Dcc_S^{SE} mutants (Figures 3A and 3B, after 24 h of incubation). The reduction of Dcc_S^{SE} axon growth was less severe than the 85% decrease we previously observed in *Dcc* knockout (KO) mutants.[33] As Netrin1 functions as both diffusible and substrate-bound factors,[38-40] we also tested DSC axon outgrowth on 2D surfaces coated with Netrin1, as previously described.[38] We found that, in response to substrate-bound Netrin1, sole expression of Dcc_L and Dcc_S also promoted and dampened axon outgrowth, respectively (Figures 3C and 3D). By contrast, baseline axon growth that is independent of Netrin1 requires a longer incubation period of 40 h in 3D collagen and was comparable between either isoform mutant and WT controls (Figure S3). Taken together, DCC isoforms have distinct growth-promoting activities in response to Netrin1 *in vitro*, consistent with their differential abilities to activate ERK1/2 (Figures 1D and 1E).

To analyze axon growth and ventral projection in an intact environment, we pulse labeled commissural neurons by electroporating a *Gfp* reporter unilaterally into the DSC, cultured the whole embryos for 36 h (from E10 to the equivalent of E11.5), and examined axon trajectories in an open-book orientation. We found that, after 36 h, WT axons were able to enter and exit the FP, and to make a sharp turn into the longitudinal axis on the contralateral side (Figure 3E). In contrast, Dcc_L^{SE} axons entered the FP normally, but most did not exit, stalling inside or at the contralateral edge of the FP. By the end of culturing, few Dcc_S^{SE} axons had reached or entered the FP (Figure 3E). Thus, consistent with the explant assays (Figures 3A-3D), Dcc_L^{SE} axons have robust growth but often fail to exit the FP. Dcc_S^{SE} axons, by contrast, have reduced growth and likely reduced entry into the FP.

We further traced axon trajectories around the midline by unilaterally injecting DiI, a membrane dye, into the spinal cord in the open-book configuration. At E11.5, DiI-labeled Dcc_L^{SE} axons entered the FP normally, but the majority failed to exit (Figure 4), consistent with the observations from GFP pulse labeling (Figure 3E). We also noticed that most Dcc_L^{SE} axons were present in bundles, which is suggestive of elevated fasciculation. A similar phenotype is present when Netrin1 is expressed from the FP alone, which is more diffusible than Netrin1 present in the ventricular zone.[39] *Netrin1* and *Dcc* KO axons, in contrast, are severely defasciculated[35,41] (also see Figure 7A). These data are consistent with

a structure study showing that Netrin1 together with Draxin mediate axon fasciculation by inducing DCC trans-interaction[42] (also see the “discussion”).

In *Dcc*$_S^{SE}$ mutants, DiI tracing revealed that a significant amount of axons stalled before entering the midline at E11.5 (Figure 4), which is also consistent with the observations from GFP pulse labeling (Figure 3E). In several mutants with deficient Netrin1/DCC signaling, including in *Dcc* KOs and conditional deletion mutants of FP Netrin1, the deficit in axon midline crossing is alleviated at later stages (i.e., midline crossing is delayed).[33,39] We thus examined *Dcc*$_S^{SE}$ mutants a day later at E12.5 and indeed found more axons being able to enter and cross the FP at the later time point (Figure S4A). 12% of *Dcc*$_S^{SE}$ axons were still blocked from entering at E12.5 and abnormally turned longitudinally on the ipsilateral side compared with just 4% in WT controls (Figure S4B). Thus, *Dcc*$_S^{SE}$ mutations significantly delay, and to a smaller degree block, midline entry.

Using commissural axon marker anti-ROBO3, we examined the thickness of the ventral commissure, which consists of midline-crossing axons. We found that, at E11.5, the ventral commissure was thicker in *Dcc*$_L^{SE}$ embryos than in WT controls and the axons appeared to accumulate in the vicinity of the FP (Figure 5). By contrast, the ventral commissure was reduced by 18% in *Dcc*$_S^{SE}$ mutants at E11.5 (Figure 5), which was less severe than the 67% reduction in *Dcc* KO mutants.[33] Examinations using additional axon markers, including anti-TAG1 and anti-ROBO3.1 (a ROBO3 isoform that is restricted to pre-crossing axonal domains[26]) confirmed that the ventral commissure was increased and decreased, respectively, in *Dcc*$_L^{SE}$ and *Dcc*$_S^{SE}$ mutants (Figures S5A-S5D). The decrease in *Dcc*$_S^{SE}$ mutants was no longer significant at the later stage of E12.5 (Figures S5E and S5F).

Together, the axon outgrowth, GFP pulse labeling, DiI tracing, and immunohistochemistry assays show that *Dcc*$_L^{SE}$ mutants are likely to have elevated Netrin1-induced activity, which promotes axon growth but causes the axons to linger within the FP. On the other hand, the severity of *Dcc*$_S^{SE}$ mutant deficits is indicative of partial loss of DCC activity, which reduces axon growth and delays midline entry. Consistent with this idea, *Dcc*$_S^{SE}$ mutant axons did not invade the motor column at a significant level or become defasciculated, both of which are observed in *Dcc* KO axons.[35,44] *Dcc*$_S^{SE}$ mutants, as well as *Dcc*$_L^{SE}$ mice, are also viable until adulthood, unlike the perinatal lethal *Dcc* KO allele.[44]

As *Dcc* isoforms are present at comparable levels during the peak of midline crossing (Figures 1B and 1C), we generated transheterozygous *Dcc*$_L^{SE}$*; Dcc*$_S^{SE}$ mutants and found that the axons entered and exited the midline normally as in WT controls by DiI tracing (Figure 4). The size of the ventral commissure in the transheterozygotes was comparable with that in WT embryos by anti-ROBO3 and anti-TAG1 staining (Figures 5, S5A, and S5B). Thus, the abnormalities present in the isoform mutants are unlikely to result from off-target mutations. Instead, both isoforms are required for proper entry and exit of the FP by commissural axons.

ROBO1 expression is unaffected in *Dcc* isoform mutants and ROBO1 interacts similarly with DCC isoforms

Failed midline exit seen in Dcc_L^{SE} embryos also occurs in mutants where SLIT/ROBO signaling is deficient[24,45] (also see Figure 7G for $Robo1^{-/-}$ mutants). We thus examined *Robo1* expression in *Dcc* isoform mutants and found that the mRNA level, alternative isoform production, and protein distribution were undisturbed (Figures 6A and S6). *Robo2* expression also was not affected (Figures 6A and S6A).

We also compared the binding between DCC isoforms and ROBO1 by co-immunoprecipitation (coIP) in cultured COS-1 cells. We found that ROBO1 interacted with either DCC_L or DCC_S in the absence of Netrin1 and SLIT2N (the N-terminal fragment[2]), and the binding with the isoforms was comparable (Figures 6B-6D). Addition of the ligands did not alter the binding of ROBO1 with either DCC isoform (Figures 6B-6D). Thus, ROBO1 binds non-discriminatorily to DCC isoforms and the binding is not gated by either ligand.

These results suggest that, despite the normal expression of ROBO1 and binding by ROBO1, expressing DCC_L alone appears to overcome midline repulsion causing the axons to linger at the FP. Furthermore, as the abnormality is similarly present in mutants deficient in SLIT/ROBO signaling,[24,45] expressing DCC_L alone also could dampen SLIT/ROBO repulsion.

Normal midline entry and exit require a balance between DCC and ROBO1 signaling

If midline stalling in Dcc_L^{SE} mutants indeed results from abnormally elevated DCC activity, which overcomes ROBO1 repulsion, then reducing DCC signaling and/or elevating ROBO1 activity should ameliorate the deficit. We thus wondered whether reducing *Robo3* activity could have a rescuing effect. When we introduced a heterozygous *Robo3* null allele, which by itself does not have a significant guidance defect,[7,18,43] into Dcc_L^{SE} mutants, most $Dcc_L^{SE}; Robo3^{+/-}$ compound mutant axons entered and exited the midline normally by DiI tracing (Figure 4). The commissure size also became comparable with that in WT controls (Figure 5). By contrast, when *Robo3* dose was reduced in Dcc_S^{SE} mutants, midline entry of DiI-labeled axons was further blocked, resulting in 25% of the axons abnormally turning longitudinally on the ipsilateral side in $Dcc_S^{SE}; Robo3^{+/-}$ embryos compared with 12% in Dcc_S^{SE} mutants at E12.5 (Figure S4). The ventral commissure size was also further reduced (Figure 5).

If modifying the strength of DCC and/or ROBO signaling can alter axonal responses to the midline, then DCC and ROBO1 may engage in opposing actions akin to a tug of war to determine the outcome of attraction vs. repulsion *in vivo*. We thus further investigated whether Netrin1/DCC signaling indeed directly counteracts SLIT/ROBO1 activity during midline entry. In $Netrin1^{-/-}$ mutants, the ventral commissure is almost completely absent due to multiple errors in the ventral projection of commissural axons, including misprojections into ectopic regions in the spinal cord (e.g., the roof plate, ventricular zone, and motor columns), as well as abnormal exits of the CNS along the dorsal and ventral roots[38,46-48] (Figure 7A). When we introduced homozygous *Robo1* deletions into *Netrin1*

null mutants, we found a small but significant increase in the ventral commissure size, by anti-ROBO3, anti-TAG1, and anti-neurofilament (NF) staining (Figures 7A, 7B, and S7). This suggests that commissural axons are responsive to SLIT/ROBO1-mediated repulsion before midline entry, which can block crossing if not repressed by Netrin1/DCC signaling. Given that *Robo3* also antagonizes *Robo1* to allow midline entry,[18,45] and that ROBO3A.1 binds DCC to potentiate attraction,[27] the same DCC/ROBO3A.1 molecular complex may inhibit ROBO1 repulsion as well.

It is important to note that deleting *Robo1* in *Netrin1* null mutants did not rectify all guidance abnormalities, as *Netrin1*$^{-/-}$*; Robo1*$^{-/-}$ axons still misprojected into ectopic regions of the spinal cord and sometimes exited the CNS (Figure 7A). Hence, in addition to opposing ROBO1 repulsion, Netrin1 is also critical in confining commissural axons within the spinal cord and in channeling the axons toward the FP.

Previous studies using explant cultures did not detect repulsive responses by pre-crossing commissural axons to SLIT2N that is secreted from cell aggregates,[17,18] leading to the notion that pre-crossing axons are nonresponsive to SLIT. We reexamined the effect of SLIT2N on pre-crossing axons using a high concentration of bath-applied SLIT2N (at 250 ng/mL) and found that DSC axons were inhibited in their outgrowth (Figures 7C-7F). For WT axons, Netrin1-independent baseline axon growth was inhibited by 71%, whereas *Robo1*$^{-/-}$*; Robo2*$^{-/-}$ double-mutant axons were not inhibited (Figures 7C and 7E). In the presence of Netrin1, which allows the axons to grow out within a shorter period of culturing, SLIT2N also reduced pre-crossing axon growth by 43% in WT controls. *Robo1*$^{-/-}$*; Robo2*$^{-/-}$ double-mutant axons, on the other hand, were no longer inhibited (Figures 7D and 7F). Thus, consistent with our *in vivo* observations (Figures 7A and 7B), pre-crossing commissural axons are sensitive to SLIT2 inhibition through ROBO receptors *in vitro*, and Netrin1 and SLIT2 exert opposing effects on axon outgrowth.

We continued to examine whether Netrin1/DCC and SLIT/ROBO1 oppose each other during midline exit. We wondered whether midline stalling caused by *Robo1* deletion[24] could be alleviated by dampening Netrin1/DCC attraction. We thus introduced a heterozygous *Netrin1* null allele into *Robo1*$^{-/-}$ mutants. With DiI labeling, we found that more axons in *Netrin1*$^{+/-}$*; Robo1*$^{-/-}$ double mutants were able to exit the midline than in *Robo1*$^{-/-}$ single mutants (Figures 7G and 7H). These results demonstrate that commissural axons remain responsive to Netrin1 after entering the FP and that Netrin1/DCC and SLIT/ROBO1 signaling continue to antagonize each other during midline exit.

DISCUSSION

Commissural axons respond to attractive and repulsive cues throughout midline crossing

Previously, SLIT2N secreted from cell aggregates was found to only inhibit post-crossing commissural axon growth.[17] We show here that bath-applied purified SLIT2N (at 250 ng/mL, likely a much higher concentration than produced from cell aggregates) can inhibit pre-crossing axon growth as well. Similarly, while Netrin1-secreting cell aggregates fail to induce an attractive response by post-crossing axons,[16] bath-applied Netrin1 (at high concentrations, >250 ng/mL) is able to stimulate post-crossing axon growth.[49] Collectively,

these *in vitro* data suggest that commissural axons likely respond to the guidance cues at quantitatively different levels before and after crossing, which may appear in an on-off manner. Nonetheless, our *in vivo* observations highlight the fact that these axons remain sensitive to both attractive and repulsive signals throughout.

Commissural axons integrate and balance the opposing DCC and ROBO1 activities

Because of the simultaneous responses to Netrin and SLIT, commissural axons in mammals will need to integrate and balance the downstream signaling pathways. This is consistent with the findings in *C. elegans* and *Drosophila* that Netrin1/DCC and SLIT/ROBO pathways act simultaneously and independently.[50,51] Our *in vivo* data are consistent with a tug-of-war model where the relative strength between DCC and ROBO1 pathways determines the final axonal responses. For axons to enter and exit the midline normally, DCC activity needs to be sufficiently high to overcome low ROBO1 expression/repulsion, but DCC attraction cannot be too strong to overpower ROBO1 after the upregulation of the latter. Such a counteraction is also observed in callosal axons during midline crossing and in spinal motor neurons in determining their soma positions and their axonal exit point out of the CNS.[28-31]

DCC and ROBO1 share many downstream factors that regulate cytoskeletal dynamics, many of which are conserved across species. For instance, the NCK/DOCK adaptors associate with both receptors,[52,53] and with effectors that affect actin cytoskeleton, including p21-activated kinase (PAK) and GTPases (e.g., RAC/CED-10 and CDC42).[52,54-59] A number of guanine nucleotide exchange factors (GEFs) and GTPase-activating proteins (GAPs) act downstream of DCC or ROBO to control RAC/CDC42 activities, including Trio/GEF, TIAM/GEF, SOS/GEF, srGAPs (SLIT-ROBO GAPs), and Vilse/RhoGAP.[54,55,60-64] The actin regulatory protein MENA/ENA/UNC-34, as well as several families of kinases, including Abl, the Src family, and PI3K-AKT,[56-59,65-68] also mediates the activities of both receptors. We speculate that the summed activities of these signaling molecules, likely locally within subdomains of growth cones, determine axonal responses on both spatial and temporal levels. Furthermore, many of the above-mentioned molecules participate in other guidance pathways[69] and are thus likely to serve as the integrative points for divergent signals.

Multiple mechanisms help maintain proper levels of Netrin1/DCC attraction

The persistent and even increased expression of Dcc_L during commissural neuron development (Figures 1B and 1C) implies an involvement of Netrin1 signaling in post-crossing axon guidance. Indeed, Netrin1 has been shown to stimulate post-crossing axon outgrowth[49] and to direct the lateral positioning of post-crossing commissural axons in the hindbrain.[70] If DCC_L remains active at the later stages, how is midline attraction kept in check to allow contralateral exit and to prevent reentry? Our data show that when attraction becomes inappropriately elevated in Dcc_L^{SE} mutants, ROBO1 upregulation alone is not sufficient to counter it. Thus, additional mechanisms are in play to help maintain proper levels of attraction.

First, the continued presence of DCC_S, although at decreasing levels over time, is most likely to be required to moderate attraction. The temporal change in the relative expression

of DCC isoforms (Figures 1B and 1C) is likely to be important in fine-tuning the strength of midline attraction, although further expression studies on the protein level and at single-axon resolution are needed.

Second, as ROBO3 dosage can affect the outcome of DCC and ROBO1 counteraction (Figures 4 and 5), the exclusion of ROBO3.1 from post-crossing axonal domains will be necessary to allow upregulated ROBO1 to antagonize DCC attraction. Consistently, we have previously shown that uniform expression of ROBO3.1 throughout the axons via electroporating a *Robo3A.1* expression plasmid in cultured WT embryos causes the axons to recross the midline.[26] Our data also suggest that the function of ROBO3 in potentiating DCC attraction and in inhibiting ROBO1 repulsion may be one unified function, at least in the spinal cord, which is to favor DCC in the tug of war. In the hindbrain pontine neurons, ROBO3 has been shown to primarily facilitate DCC attraction.[27] Whether Netrin1/DCC_L also opposes ROBO repulsion in these hindbrain neurons remains to be investigated.

Furthermore, *in vivo* studies of spinal motor axons have uncovered additional mechanisms in achieving proper control of Netrin1 attraction. In these axons, attraction toward Netrin1 at the midline and at the basement membrane is initially kept low to allow the axons to exit the spinal cord, but attraction becomes upregulated later toward muscle-derived Netrin1 to facilitate innervation. p190RhoGAP has been shown to transiently bind and inactivate DCC as the motor axons exit the CNS, and the exit is abnormally blocked in $p190^{-/-}$ mutants.[71] In addition, cleavage of DCC by γ-secretase, after DCC ectodomain shedding, is required to control Netrin1 attraction in both motor and commissural axons. Loss of the Presenilin 1 subunit of γ-secretase leads to the accumulation of a membrane-tethered DCC intracellular domain (i.e., the DCC stub), which abnormally elevates attraction.[72] Consequently, motor axons inappropriately cross the midline and commissural axons stall within the midline or recross. As the DCC stub can bind full-length DCC but not ROBO1, it is hypothesized that the DCC stub blocks full-length DCC from dimerizing with ROBO1 and becoming silenced. It is interesting to note that, in *C. elegans*, where *Unc-40/Dcc* and *Sax-3/Robo* function independently, a myristoylated and membrane-tethered UNC-40/DCC intracellular domain acts as a gain-of-function mutant.[58] Therefore, the DCC stub may elevate DCC attraction independent of ROBO1 action.

Midline entry is delayed when Netrin1/DCC signaling is deficient

A temporal delay in midline entry is consistently observed in mutants with dampened Netrin1/DCC activity.[33,39] The tug-of-war model provides a plausible explanation for this phenomenon, which is based on our finding of a temporal change in the opposing ROBO1 signaling.[43] We have previously shown that *Robo1* undergoes NOVA-controlled alternative splicing during commissural neuron development to generate the e6b+ and e6b− isoforms, which includes and excludes microexon 6b, respectively.[43] The mRNA level of the more repulsive e6b+ isoform decreases over development relative to e6b−[43] (also see Figure S6B), suggesting that while ROBO1 protein level remains low and constant pre-crossing, its repulsive activity may be decreasing. Consistent with this notion, we show that deleting the e6b+ isoform *in vivo* allows commissural axons to arrive at the midline earlier than in WT embryos.[43] Therefore, it is possible that commissural axons with dampened DCC attraction

are only able to enter the midline once ROBO1 repulsion has become sufficiently low as a result of decreasing e6b+ expression. *In vivo* studies are needed to examine this hypothesis.

Multiple signaling pathways may participate in the tug of war during midline exit

Besides SLIT/ROBO signaling, semaphorins/Neuropilin1[17] and SLIT2(C-term)/PlexinA1[73] pathways are also required to promote midline exit. Loss of any of these signals leads to axon stalling at the midline, suggesting that they act in a nonredundant manner. The tug-of-war model would still stand when considering these additional molecules, in that the repulsive signals would jointly counteract DCC to allow midline exit and losing any of them would similarly cause DCC to overpower repulsion.

Netrin1-DCC-mediated axon fasciculation

Besides inducing *cis* interaction between DCC,[35] soluble Netrin1 together with Draxin also mediate DCC *trans* interaction to facilitate axon fasciculation.[42] Consistently, expressing only floor-plate-derived diffusible Netrin1 elevates axon adhesion, causing commissural axons to form compact bundles.[39] As both DCC isoforms contain the Netrin1-and Draxin-binding domains involved in *trans* interaction, the isoforms are expected to be able to form homo-*trans* dimers as well as hetero-*trans* dimers. Indeed, we found that commissural axons in both isoform mutants are able to fasciculate, unlikely in *Dcc* KO embryos, and DCCL sole expression caused hyperfasciculation. This suggests that DCC_L may form a higher amount of homo-*trans* dimers than DCCs does, as the latter assembles into high-molecular-weight oligomers in *cis*.[35] Nonetheless, the ability of DCCs to maintain axon adhesion likely contributes to the incomplete loss of function in Dcc_S^{SE} mutants.

Limitations of the study

In the current study, the detection of *Dcc* isoforms is performed at the mRNA level due to the lack of isoform-specific antibodies. The resolution of the isoform expression is at the population level, where mixed DSC neurons were collectively analyzed. Therefore, future studies at the protein level and at single-neuron resolution will be necessary to investigate the spatial and temporal production of the DCC receptor variants.

STAR★METHODS

RESOURCE AVAILABILITY

Lead contact—Inquiries about methods, reagents, or data availability should be addressed to Dr. Zhe Chen (chen6867@umn.edu).

Materials availability—The transgenic mouse models and recombinant DNA constructs that were produced in this study will be made available after completion of a Material Transfer Agreement. Requests for these materials should be addressed to the lead contact.

Data and code availability

- All data reported in this paper will be shared by the lead contact upon request.
- There are no original codes generated in this paper.

- Any additional information required to reanalyze the data reported in this paper is available from the lead contact upon request.

EXPERIMENTAL MODEL AND SUBJECT DETAILS

Mouse lines—*Netrin1*$^{-/-}$, *Robo1*$^{-/-}$, *Robo1*$^{-/-}$; *Robo2*$^{-/-}$, and *Robo3*$^{-/-}$ mutants have been previously characterized.[18,24,26,47] All mutants have been outbred with the CD-1 strain. *Dcc*$_L^{SE}$ and *Dcc*$_S^{SE}$ mutants were generated from pro-nuclear injection of one-cell mouse embryos from the FVB strain and have been outbred with CD1 mice for at least six generations. Unlike *Dcc* knockout allele,[44] both *Dcc*$_L^{SE}$ and *Dcc*$_S^{SE}$ mutants are viable until adulthood. In all experiments, homozygous mutants and WT controls were generated from interbreeding heterozygotes. See Table S1 for sequences of genotyping oligos and PCR conditions for *Dcc* isoform mutant strains.

Ethics approval and consent to participate—All experimental manipulations and care of mice have been approved by the Institutional Animal Care and Use Committee at the University of Colorado Boulder and the University of Minnesota Medical School.

METHOD DETAILS

CRISPR-Cas9-mediated mutagenesis—Guide RNAs (gRNAs) targeting nucleotides at or near the two splice acceptor sites were designed and synthesized by Integrated DNA Technologies (IDT). A humanized coding sequence of *S. pyogenes* CAS9, amplified from pX330[74] (42230, Addgene), was cloned into pJET1.2 (ThermoFisher Scientific) and was *in vitro* transcribed using MEGAscriptT7 Transcription Kit (AMB13345, ThermoFisher Scientific). The mRNA product was purified using MEGAclear transcription cleanup kit (AM1908, ThermoFisher Scientific). Pronuclear injection was performed by the Transgenic Facility at the Department of MCDB at the University of Colorado Boulder. RNAs were injected at 100 ng/μl for *Cas9* mRNA and 25 ng/μl for guide RNA in injection buffer (1 mM Tris HCl, pH 7.5, 0.1 mM EDTA, prepared with RNase- and Dnase-free water).

Using PCR amplification and Sanger sequencing, we identified genomic mutations within the targeted regions (see Figure S1). To screen for desired mutations, we introduced the same mutations into a splicing reporter construct containing *Dcc* genomic sequences from exons 16 to 17.[33] The reporter construct was transfected into COS-1 cells (ATCC) and the resulting alternative splicing pattern was determined by semi-quantitative RT-PCR and gel electrophoresis. Mutations that led to sole expression of either isoform were selected and mice harboring these desired mutations were further outbred.

To examine *Dcc* alternative splicing *in vivo*, we performed semi-quantitative RT-PCR and gel electrophoresis using homozygous mutant tissues. In addition, we cloned the RT-PCR products between exons 16 and 23 into pCR2.1 TOPO cloning vector (Invitrogen), and Sanger sequenced ~40 clones for each founder mouse line. We did not detect any product that was generated from utilizing cryptic splice sites including the sites we have previously identified.[33] Both *Dcc*$_S^{SE}$ lines introduced mutations to the first 60 nt of exon 17 and could have affected *Dcc*$_L$ coding sequence. However, we did not detect any RT-PCR product that

contained sequences from the 60 nt in Dcc_S^{SE} mutants. Therefore, the genomic mutations in all CRISPR-Cas9 mutants affected *Dcc* on the alternative splicing level.

Quantitative and semi-quantitative RT-PCR—The spinal cord was microdissected, and the dorsal and ventral halves were separated to differentiate the dorsal commissural population from the ventral motor population. Rat tissues were used to examine isoform expression from E11 to E15 (equivalent to E9.5 to E13.5 in mice) to allow separation of dorsal spinal cord at the very early embryonic stages. Total RNA was extracted using Trizol reagent (ThermoFisher Scientific) and reverse transcription was performed using Maxima RT enzyme (ThermoFisher Scientific). Quantitative PCR was performed with a CFX Connect Real-Time PCR Detection System (BioRad). Semi-quantitative PCR was performed to simultaneously amplify different isoforms in a single reaction and to compare the relative expression by gel electrophoresis. The cycle number used in semi-quantitative PCR was determined by quantitative PCR to obtain products during the exponential amplification phase.

ERK1/2 activation and western blotting—*Dcc* expression plasmid was transfected into cultured COS-1 cells with TransitLT1 transfection reagent (Mirus Bio) (100 ng DNA/well, 24 well culture plate, 50-80% confluency). 24 h post-transfection, the cells were stimulated with 250 ng/ml Netrin1 (1109-N1, R&D) for the indicated durations. We have found that longer transfection and higher amount of transfected DNA reduced ERK1/2 activation. The cells were lysed with 10 mM Tris, pH 7.4,500 mM NaCl, 1% Triton X-100, with protease and phosphatase inhibitors (the high salt and detergent concentrations were used to help release nuclear-localized ERK1/2). After centrifugation to remove insoluble materials, SDS-containing sample buffer (with 1 mM DTT) was added to the cleared lysate. Samples were denatured at 70°C for 10 min and analyzed by SDS-PAGE and western blotting. Antibodies used for western blotting were phospho-ERK1/2 (Thr202/yr204, 9101, Cell Signaling Technology), total ERK1/2 (9102, CST), HRP-conjugated anti-Rabbit (111-035-144, Jackson ImmunoResearch), and HRP-conjugated anti-HA (3F10, Roche). Chemiluminescent signals were generated using SuperSignal West Femto maximum sensitivity substrate (34094, ThermoFisher) and acquired with ChemiDoc Imaging System (BioRad). The signal intensity was measured with ImageJ (NIH) and quantification was performed using results from three independent experiments. The phospho- to total ERK1/2 ratio was normalized to time point 0 for each experiment.

Western blotting for detecting DCC—The spinal cord was microdissected and lysed in 8 M urea, 10 mM Tris, pH 7.4 (the buffer was used to help dissolve DCC_S, which has been shown to form high molecular weight oligomers with Netrin1[35]). After clearing the lysate by centrifugation, SDS-containing sample buffer (with 1 mM DTT) was added to the supernatant. Samples were denatured at 70°C for 10 min and analyzed by SDS-PAGE and western blotting. DCC was detected with a mouse monoclonal antibody against the intracellular domain (Clone 531505, MAB5884, Novus Biologicals), and then with HRP-conjugated mouse TrueBlot Ultra secondary antibody (18-8817-30, Rockland). βActin level, measured by anti-βActin-HRP (A3854, Sigma) was used for loading control. Chemiluminescent signals were generated using SuperSignal West Femto maximum

sensitivity substrate (34094, ThermoFisher) and were acquired with ChemiDoc Imaging System (BioRad).

3D and 2D dorsal spinal cord (DSC) explant cultures—DSC was microdissected from E11.5 mouse embryos and cut into small pieces (~150-200 μm in width/length). For 3D cultures, DSC was embedded in collagen (rat-tail collagen I, 354236, Corning, diluted to 1 mg/ml with the culture medium for gelling). The explants were cultured in DMEM/F12 supplemented with 10% FBS, 1% D-glucose, 1 mM L-glutamine, 100 units/ml penicillin, and 100 μg/ml streptomycin at 37°C. The explants were cultured for 24 and 40 h in the presence and absence of Netrin1, respectively. Netrin1 (1109-N1, R&D) and SLIT2 (N-term, 757104, BioLegend) were bath-applied at the indicated concentrations in figures.

For 2D cultures, the surface of culture wells (Nunc Lab-Tek II 8-well chamber slide, 154534PK, ThermoFisher) was coated with 10 μg/ml poly-D-lysine (A3890401, ThermoFisher) and 2 μg/ml Netrin1 (1109-N1, R&D) as previously describe.[38] The explants were cultured in Neurobasal Plus medium supplemented with 2% B-27 Plus, 2 mM glutamine, 100 units/ml penicillin, 100 μg/ml streptomycin, 0.5% methyl-cellulose, and 0.75% D-glucose at 37°C for 24 h.

After fixation with 4% paraformaldehyde (PFA), the explants were stained with anti-β-TubulinIII (T3952, Sigma-Aldrich) and Alexa Fluor 594-conjugated secondary antibodies (Jackson ImmunoResearch). The fluorescent signals were measured with ImageJ (NIH). The outgrowth was quantified as the ratio between the signals from the axons and from the somas after background extraction. 3–5 explants from each embryo were quantified, with genotypes and treatments blinded.

Whole embryo culture (WEC)—Whole mouse embryos were microdissected at E10, with the yolk sac and the amnion torn open but still attached. An *Actb-gfp* plasmid, pCAG-GFP, was microinjected into the ventricle of the neural tube and electroporated into one side of the spinal cord using ECM 830 squarewave electroporation system (BTX, 30V, 50 ms each pulse, 5 pulses, plasmid DNA used at 100 ng/ml). We have previously shown that the neurons/axons labeled by *Actb-gfp* at this stage are the commissural populations using various markers.[33]

We have previously found that it takes about 26 h for spinal interneuron progenitors to migrate radially out of the ventricular zone and to turn into the D-V orientation as they continue to migrate tangentially.[76] We have also shown that after 40 h, WT axons have mostly crossed the midline and many have reached the lateral funiculi at a distance away.[43] We therefore selected 36 h of culturing, a time point when most WT axons are likely to be navigating around the midline. Also for technical reasons, openbook spinal cords that are younger than E11.5 are difficult to prepare. We thus set the end point at E11.5 and started the electroporation 36 h prior.

The embryos were cultured in growth medium [whole embryo culture rat serum (B.4520, Envigo), 10 mM D-glucose, 2 mM L-glutamine, 100 units/ml penicillin, and 100 μg/ml streptomycin] at 37°C. The embryos were grown in a precision incubator (BTC engineering,

Milton, England) with 60% O_2/5% CO_2 supplied during the first 12 h (until the equivalent of E10.5) and with 95% O_2/5% CO_2 for another 24 h (the equivalent of E10.5 to E11.5). The spinal cords were microdissected, fixed in an openbook configuration with 4% PFA overnight at 4°C, and then imaged with fluorescence microscopy.

DiI tracing—The spinal cord was microdissected in an openbook configuration and was fixed with 4% PFA. Vybrant DiI solution (V22885, ThermoFisher Scientific) was microinjected into one side of the spinal cord at mediodorsal positions, and the sample was incubated overnight at 37°C in 0.1 M PBS. Z-stack images were acquired on a Keyence All-in-One fluorescence microscope BZ-X800, at a step size of 0.5-1.0 μm. Maximum intensity Z-projections were then generated from consecutive optical sections. DiI signals were measured using ImageJ around the ipsilateral and contralateral boundaries of the floorplate to represent midline entry and exit, respectively (see Figures 4B and 4C). 3-5 injection points were analyzed for each embryo.

Immunohistochemistry (IHC) and whole mount staining—Embryos of the indicated ages were collected and fixed with 4% PFA. After being cryopreserved in 30% sucrose, the samples were embedded in OCT (Optimal Cutting Temperature) and 20 μm thick sections were collected using a cryostat (CM3050s, Leica). Antibodies used for IHC are as follows: anti-DCC (AF844, R&D), anti-ROBO1 (AF1749, R&D), anti-ROBO2 (E4M6D, Cell Signaling Technology), anti-ROBO3,[18] anti-ROBO3.1,[26] anti-TAG1 (AF4439, R&D), anti-NF (2H3, DSHB), and Alexa Fluor 594-conjugated secondary antibodies (Jackson ImmunoResearch). Antibodies were used at final concentrations of 0.5-1 μg/ml and were diluted in 0.1 M PBS, 0.1% Triton X-100, and 5% donkey serum.

The ventral commissure size was measured as the ratio between the thickness of the commissure and the height of the floor plate cells. Measurements were made using ImageJ. To minimize developmental variations, we examined embryos from different litters and of comparable sizes. 5-10 spinal cord sections taken from the brachial level were quantified for each embryo, with the genotypes blinded.

For whole mount staining, the spinal cord was microdissected and fixed in 4% PFA in an openbook configuration. The tissue was permeabilized and blocked with 0.1 M PBS, 0.2% Triton x100, and 5% donkey serum. The same buffer was used for incubation with anti-ROBO3,[18] Alexa Fluor 594-conjugated secondary antibody, and for washes in between. Anti-ROBO3 was used at 1 μg/ml. Z-stack images were acquired on a Keyence All-in-One fluorescence microscope BZ-X800, at a step size of 1 μm. Maximum intensity Z-projections were then generated from consecutive optical sections. To quantify the amount of axons crossing the midline, the signal from a selected area within the floorplate, measured with ImageJ, was compared to that from an adjacent same-sized area from the ventral spinal cord (see Figure S7A).

Co-immunoprecipitation (coIP)—*Dcc* and *Robo1(e6b+)* coding sequences were tagged with HA and V5 peptide sequences at the C-terminal end, respectively. The expression plasmids were co-transfected at 1:1 ratio into cultured COS-1 cells with TransitLT1 transfection reagent (Mirus Bio) (100 ng DNA/plasmid/well, 24 well culture plate, 50-80%

confluency). 24 h post-transfection, the cells were stimulated with 250 ng/ml Netrin1 (1109-N1, R&D) and 250 ng/ml SLIT2 (N-term, 757104, BioLegend) for 30 min. The cells were lysed in 10 mM Tris, pH 7.4, 150 mM NaCl, 0.1% Triton X100, with protease inhibitors (A32953, ThermoFisher Scientific). After clearing the lysate by centrifugation, half of the lysate was incubated with anti-HA resins (11815016001, Roche) and the other half with anti-V5 beads (ab1229, Abcam). After extensive washing, SDS-containing sample buffer (with 1 mM DTT) was added to the precipitated beads. The samples were denatured at 70°C for 10 min and analyzed by SDS-PAGE and western blotting. Antibodies used for western blotting were HRP-conjugated anti-HA (3F10, Roche) and HRP-conjugated anti-V5 (R96125, ThermoFisher Scientific). Chemiluminescent signals were generated using SuperSignal West Femto maximum sensitivity substrate (34094, ThermoFisher) and acquired with ChemiDoc Imaging System (BioRad). The signal intensity was measured with ImageJ (NIH). The signals from immunoprecipitation (IP) and immunoblotting (IB) using the same antibody are considered as the input. The signals obtained from IP and IB with different antibodies, e.g., IP with anti-V5 and IB with anti-HA, are considered as the coIP fraction. The ratio between coIP and input signals were then normalized to lane 1 (i.e., DCC_L-HA+ ROBO1-V5, no ligand) for each experiment to represent the level of interaction between DCC and ROBO1. Quantification was performed using results from three independent experiments.

QUANTIFICATION AND STATISTICAL ANALYSIS

Statistical analyses were performed using GraphPad Prism 9. All data are presented as mean ± SD. p values, animal numbers, and the statistical tests are stated in graphs or figure legends.

Supplementary Material

Refer to Web version on PubMed Central for supplementary material.

ACKNOWLEDGMENTS

This work was supported by the following grants: Masonic Institute for the Developing Brain grant (Z.C.); National Institutes of Health (NIH) R21DA056728 (Z.C.); and NIH R01EY024261 and R01EY033316 (H.J.J.). We thank Yudong Teng at MCDB transgenic facility at the University of Colorado Boulder for generating CRISPR-Cas9-mediated mutant mice, Kelsey R. Arbogast for technical assistance, and Linda McLoon and Yasushi Nakagawa for critical comments on the manuscript. The graphic abstract was created with BioRender.com.

REFERENCES

1. Serafini T, Kennedy TE, Galko MJ, Mirzayan C, Jessell TM, and Tessier-Lavigne M (1994). The netrins define a family of axon outgrowth-promoting proteins homologous to C. elegans UNC-6. Cell 78, 409–424. [PubMed: 8062384]
2. Brose K, Bland KS, Wang KH, Arnott D, Henzel W, Goodman CS, Tessier-Lavigne M, and Kidd T (1999). Slit proteins bind Robo receptors and have an evolutionarily conserved role in repulsive axon guidance. Cell 96, 795–806. [PubMed: 10102268]
3. Butler SJ, and Dodd J (2003). A role for BMP heterodimers in roof plate-mediated repulsion of commissural axons. Neuron 38, 389–401. [PubMed: 12741987]
4. Augsburger A, Schuchardt A, Hoskins S, Dodd J, and Butler S (1999). BMPs as mediators of roof plate repulsion of commissural neurons. Neuron 24, 127–141. [PubMed: 10677032]

5. Charron F, Stein E, Jeong J, McMahon AP, and Tessier-Lavigne M (2003). The morphogen sonic hedgehog is an axonal chemoattractant that collaborates with netrin-1 in midline axon guidance. Cell 113, 11–23. [PubMed: 12679031]
6. Ruiz de Almodovar C, Fabre PJ, Knevels E, Coulon C, Segura I, Haddick PCG, Aerts L, Delattin N, Strasser G, Oh W-J, et al. (2011). VEGF mediates commissural axon chemoattraction through its receptor Flk1. Neuron 70, 966–978. 10.1016/j.neuron.2011.04.014. [PubMed: 21658588]
7. Jaworski A, Tom I, Tong RK, Gildea HK, Koch AW, Gonzalez LC, and Tessier-Lavigne M (2015). Operational redundancy in axon guidance through the multifunctional receptor Robo3 and its ligand NELL2. Science 350, 961–965. 10.1126/science.aad2615. [PubMed: 26586761]
8. Islam SM, Shinmyo Y, Okafuji T, Su Y, Naser IB, Ahmed G, Zhang S, Chen S, Ohta K, Kiyonari H, et al. (2009). Draxin, a repulsive guidance protein for spinal cord and forebrain commissures. Science 323, 388–393. 10.1126/science.1165187. [PubMed: 19150847]
9. Morales D, and Kania A (2017). Cooperation and crosstalk in axon guidance cue integration: Additivity, synergy, and fine-tuning in combinatorial signaling. Dev. Neurobiol 77, 891–904. 10.1002/dneu.22463. [PubMed: 27739221]
10. Lai Wing Sun K, Correia JP, and Kennedy TE (2011). Netrins: Versatile extracellular cues with diverse functions. Development 138, 2153–2169. 10.1242/dev.044529. [PubMed: 21558366]
11. Ypsilanti AR, and Chedotal A (2014). ROUNDABOUT receptors. In Cell Adhesion Molecules: Implications in Neurological Diseases, Berezin V and Walmod PS, eds. (Springer), pp. 133–164. 10.1007/978-1-4614-8090-7_7.
12. Ballard MS, and Hinck L (2012). A roundabout way to cancer. Adv. Cancer Res 114, 187–235. 10.1016/B978-0-12-386503-8.00005-3. [PubMed: 22588058]
13. Klagsbrun M, and Eichmann A (2005). A role for axon guidance receptors and ligands in blood vessel development and tumor angiogenesis. Cytokine Growth Factor Rev. 16, 535–548. [PubMed: 15979925]
14. Dickson BJ, and Zou Y (2010). Navigating intermediate targets: The nervous system midline. Cold Spring Harbor Perspect. Biol 2, a002055. 10.1101/cshperspect.a002055.
15. Evans TA, and Bashaw GJ (2010). Axon guidance at the midline: Of mice and flies. Curr. Opin. Neurobiol 20, 79–85. 10.1016/j.conb.2009.12.006. [PubMed: 20074930]
16. Shirasaki R, Katsumata R, and Murakami F (1998). Change in chemoattractant responsiveness of developing axons at an intermediate target. Science 279, 105–107. [PubMed: 9417018]
17. Zou Y, Stoeckli E, Chen H, and Tessier-Lavigne M (2000). Squeezing axons out of the gray matter: A role for slit and semaphorin proteins from midline and ventral spinal cord. Cell 102, 363–375. [PubMed: 10975526]
18. Sabatier C, Plump AS, Le M, Brose K, Tamada A, Murakami F, Lee EY, and Tessier-Lavigne M (2004). The divergent Robo family protein rig-1/Robo3 is a negative regulator of slit responsiveness required for midline crossing by commissural axons. Cell 117, 157–169. [PubMed: 15084255]
19. Justice ED, Barnum SJ, and Kidd T (2017). The WAGR syndrome gene PRRG4 is a functional homologue of the commissure less axon guidance gene. PLoS Genet. 13, e1006865. 10.1371/journal.pgen.1006865. [PubMed: 28859078]
20. Gorla M, Santiago C, Chaudhari K, Layman AAK, Oliver PM, and Bashaw GJ (2019). Ndfip proteins target Robo receptors for degradation and allow commissural axons to cross the midline in the developing spinal cord. Cell Rep. 26, 3298–3312.e4. 10.1016/j.celrep.2019.02.080. [PubMed: 30893602]
21. Yang T, Huang H, Shao Q, Yee S, Majumder T, and Liu G (2018). miR-92 suppresses Robo1 translation to modulate slit sensitivity in commissural axon guidance. Cell Rep. 24, 2694–2708.e6. 10.1016/j.celrep.2018.08.021. [PubMed: 30184503]
22. Alther TA, Domanitskaya E, and Stoeckli ET (2016). Calsyntenin 1-mediated trafficking of axon guidance receptors regulates the switch in axonal responsiveness at a choice point. Development 143, 994–1004. 10.1242/dev.127449. [PubMed: 26839361]
23. Philipp M, Niederkofler V, Debrunner M, Alther T, Kunz B, and Stoeckli ET (2012). RabGDI controls axonal midline crossing by regulating Robo1 surface expression. Neural Dev. 7, 36. 10.1186/1749-8104-7-36. [PubMed: 23140504]

24. Long H, Sabatier C, Ma L, Plump A, Yuan W, Ornitz DM, Tamada A, Murakami F, Goodman CS, and Tessier-Lavigne M (2004). Conserved roles for Slit and Robo proteins in midline commissural axon guidance. Neuron 42, 213–223. [PubMed: 15091338]
25. Stein E, and Tessier-Lavigne M (2001). Hierarchical organization of guidance receptors: Silencing of netrin attraction by slit through a Robo/DCC receptor complex. Science 291, 1928–1938. [PubMed: 11239147]
26. Chen Z, Gore BB, Long H, Ma L, and Tessier-Lavigne M (2008). Alternative splicing of the Robo3 axon guidance receptor governs the midline switch from attraction to repulsion. Neuron 58, 325–332. 10.1016/j.neuron.2008.02.016. [PubMed: 18466743]
27. Zelina P, Blockus H, Zagar Y, Péres A, Friocourt F, Wu Z, Rama N, Fouquet C, Hohenester E, Tessier-Lavigne M, et al. (2014). Signaling switch of the axon guidance receptor Robo3 during vertebrate evolution. Neuron 84, 1258–1272. 10.1016/j.neuron.2014.11.004. [PubMed: 25433640]
28. Fothergill T, Donahoo A-LS, Douglass A, Zalucki O, Yuan J, Shu T, Goodhill GJ, and Richards LJ (2014). Netrin-DCC signaling regulates corpus callosum formation through attraction of pioneering axons and by modulating Slit2-mediated repulsion. Cereb. Cortex 24, 1138–1151. 10.1093/cercor/bhs395. [PubMed: 23302812]
29. Kim M, Farmer WT, Bjorke B, McMahon SA, Fabre PJ, Charron F, and Mastick GS (2014). Pioneer midbrain longitudinal axons navigate using a balance of Netrin attraction and Slit repulsion. Neural Dev. 9, 17. 10.1186/1749-8104-9-17. [PubMed: 25056828]
30. Kim M, Fontelonga T, Roesener AP, Lee H, Gurung S, Mendonca PRF, and Mastick GS (2015). Motor neuron cell bodies are actively positioned by Slit/Robo repulsion and Netrin/DCC attraction. Dev. Biol 399, 68–79. 10.1016/j.ydbio.2014.12.014. [PubMed: 25530182]
31. Kim M, Fontelonga TM, Lee CH, Barnum SJ, and Mastick GS (2017). Motor axons are guided to exit points in the spinal cord by Slit and Netrin signals. Dev. Biol 432, 178–191. 10.1016/j.ydbio.2017.09.038. [PubMed: 28986144]
32. Leyva-Díaz E, Del Toro D, Menal MJ, Cambray S, Susin R, Tessier-Lavigne M, Klein R, Egea J, and López-Bendito G (2014). FLRT3 Is a Robo1-interacting protein that determines netrin-1 attraction in developing axons. Curr. Biol 24, 494–508. 10.1016/j.cub.2014.01.042. [PubMed: 24560577]
33. Leggere JC, Saito Y, Darnell RB, Tessier-Lavigne M, Junge HJ, and Chen Z (2016). NOVA regulates Dcc alternative splicing during neuronal migration and axon guidance in the spinal cord. Elife 5, e14264. 10.7554/eLife.14264. [PubMed: 27223328]
34. Saito Y, Miranda-Rottmann S, Ruggiu M, Park CY, Fak JJ, Zhong R, Duncan JS, Fabella BA, Junge HJ, Chen Z, et al. (2016). NOVA2-mediated RNA regulation is required for axonal pathfinding during development. Elife 5, e14371. 10.7554/eLife.14371. [PubMed: 27223325]
35. Xu K, Wu Z, Renier N, Antipenko A, Tzvetkova-Robev D, Xu Y, Minchenko M, Nardi-Dei V, Rajashankar KR, Himanen J, et al. (2014). Structures of netrin-1 bound to two receptors provide insight into its axon guidance mechanism. Science 344, 1275–1279. 10.1126/science.1255149. [PubMed: 24876346]
36. Forcet C, Stein E, Pays L, Corset V, Llambi F, Tessier-Lavigne M, and Mehlen P (2002). Netrin-1-mediated axon outgrowth requires deleted in colorectal cancer-dependent MAPK activation. Nature 417, 443–447. [PubMed: 11986622]
37. Keino-Masu K, Masu M, Hinck L, Leonardo ED, Chan SS, Culotti JG, and Tessier-Lavigne M (1996). Deleted in Colorectal Cancer (DCC) encodes a netrin receptor. Cell 87, 175–185. [PubMed: 8861902]
38. Wu Z, Makihara S, Yam PT, Teo S, Renier N, Balekoglu N, Moreno-Bravo JA, Olsen O, Chédotal A, Charron F, and Tessier-Lavigne M (2019). Long-range guidance of spinal commissural axons by Netrin1 and sonic hedgehog from midline floor plate cells. Neuron 101, 635–647.e4. 10.1016/j.neuron.2018.12.025. [PubMed: 30661738]
39. Moreno-Bravo JA, Roig Puiggros S, Mehlen P, and Chédotal A (2019). Synergistic activity of floor-plate- and ventricular-zone-derived netrin-1 in spinal cord commissural axon guidance. Neuron 101, 625–634.e3. 10.1016/j.neuron.2018.12.024. [PubMed: 30661739]
40. Varadarajan SG, Kong JH, Phan KD, Kao T-J, Panaitof SC, Cardin J, Eltzschig H, Kania A, Novitch BG, and Butler SJ (2017). Netrin1 produced by neural progenitors, not floor

plate cells, is required for axon guidance in the spinal cord. Neuron 94, 790–799.e3. 10.1016/j.neuron.2017.03.007. [PubMed: 28434801]

41. Serafini T, Colamarino SA, Leonardo ED, Wang H, Beddington R, Skarnes WC, and Tessier-Lavigne M (1996). Netrin-1 is required for commissural axon guidance in the developing vertebrate nervous system. Cell 87, 1001–1014. [PubMed: 8978605]
42. Liu Y, Bhowmick T, Liu Y, Gao X, Mertens HDT, Svergun DI, Xiao J, Zhang Y, Wang J-H, and Meijers R (2018). Structural basis for draxin-modulated axon guidance and fasciculation by netrin-1 through DCC. Neuron 97, 1261–1267.e4. 10.1016/j.neuron.2018.02.010. [PubMed: 29503192]
43. Johnson V, Junge HJ, and Chen Z (2019). Temporal regulation of axonal repulsion by alternative splicing of a conserved microexon in mammalian Robo1 and Robo2. Elife 8, e46042. 10.7554/eLife.46042. [PubMed: 31392959]
44. Fazeli A, Dickinson SL, Hermiston ML, Tighe RV, Steen RG, Small CG, Stoeckli ET, Keino-Masu K, Masu M, Rayburn H, et al. (1997). Phenotype of mice lacking functional Deleted in colorectal cancer (Dcc) gene. Nature 386, 796–804. 10.1038/386796a0. [PubMed: 9126737]
45. Jaworski A, Long H, and Tessier-Lavigne M (2010). Collaborative and specialized functions of Robo1 and Robo2 in spinal commissural axon guidance. J. Neurosci 30, 9445–9453. 10.1523/JNEUROSCI.6290-09.2010. [PubMed: 20631173]
46. Bin JM, Han D, Lai Wing Sun K, Croteau L-P, Dumontier E, Cloutier J-F, Kania A, and Kennedy TE (2015). Complete loss of netrin-1 results in embryonic lethality and severe axon guidance defects without increased neural cell death. Cell Rep. 12, 1099–1106. 10.1016/j.celrep.2015.07.028. [PubMed: 26257176]
47. Yung AR, Nishitani AM, and Goodrich LV (2015). Phenotypic analysis of mice completely lacking netrin 1. Development 142, 3686–3691. 10.1242/dev.128942. [PubMed: 26395479]
48. Laumonnerie C, Da Silva RV, Kania A, and Wilson SI (2014). Netrin 1 and Dcc signalling are required for confinement of central axons within the central nervous system. Development 141, 594–603. 10.1242/dev.099606. [PubMed: 24449837]
49. Gore BB, Wong KG, and Tessier-Lavigne M (2008). Stem cell factor functions as an outgrowth-promoting factor to enable axon exit from the midline intermediate target. Neuron 57, 501–510. 10.1016/j.neuron.2008.01.006. [PubMed: 18304480]
50. Garbe DS, and Bashaw GJ (2007). Independent functions of Slit-Robo repulsion and Netrin-Frazzled attraction regulate axon crossing at the midline in Drosophila. J. Neurosci 27, 3584–3592. 10.1523/JNEUROSCI.0301-07.2007. [PubMed: 17392474]
51. Hao JC, Yu TW, Fujisawa K, Culotti JG, Gengyo-Ando K, Mitani S, Moulder G, Barstead R, Tessier-Lavigne M, and Bargmann CI (2001). C. elegans slit acts in midline, dorsal-ventral, and anterior-posterior guidance via the SAX-3/Robo receptor. Neuron 32, 25–38. [PubMed: 11604136]
52. Fan X, Labrador JP, Hing H, and Bashaw GJ (2003). Slit stimulation recruits Dock and Pak to the roundabout receptor and increases Rac activity to regulate axon repulsion at the CNS midline. Neuron 40, 113–127. [PubMed: 14527437]
53. Li X, Meriane M, Triki I, Shekarabi M, Kennedy TE, Larose L, and Lamarche-Vane N (2002). The adaptor protein Nck-1 couples the netrin-1 receptor DCC (deleted in colorectal cancer) to the activation of the small GTPase Rac1 through an atypical mechanism. J. Biol. Chem 277, 37788–37797. 10.1074/jbc.M205428200. [PubMed: 12149262]
54. Forsthoefel DJ, Liebl EC, Kolodziej PA, and Seeger MA (2005). The abelson tyrosine kinase, the Trio GEF and enabled interact with the netrin receptor frazzled in Drosophila. Development 132, 1983–1994. [PubMed: 15790972]
55. Wong K, Ren XR, Huang YZ, Xie Y, Liu G, Saito H, Tang H, Wen L, Brady-Kalnay SM, Mei L, et al. (2001). Signal transduction in neuronal migration: Roles of GTPase activating proteins and the small GTPase Cdc42 in the Slit-Robo pathway. Cell 107, 209–221. [PubMed: 11672528]
56. Chang C, Adler CE, Krause M, Clark SG, Gertler FB, Tessier-Lavigne M, and Bargmann CI (2006). MIG-10/lamellipodin and AGE-1/PI3K promote axon guidance and outgrowth in response to slit and netrin. Curr. Biol 16, 854–862. [PubMed: 16618541]

57. Yu TW, Hao JC, Lim W, Tessier-Lavigne M, and Bargmann CI (2002). Shared receptors in axon guidance: SAX-3/Robo signals via UNC-34/Enabled and a Netrin-independent UNC-40/DCC function. Nat. Neurosci 5, 1147–1154. [PubMed: 12379860]
58. Gitai Z, Yu TW, Lundquist EA, Tessier-Lavigne M, and Bargmann CI (2003). The netrin receptor UNC-40/DCC stimulates axon attraction and outgrowth through enabled and, in parallel, Rac and UNC-115/AbLIM. Neuron 37, 53–65. [PubMed: 12526772]
59. Bashaw GJ, Kidd T, Murray D, Pawson T, and Goodman CS (2000). Repulsive axon guidance: abelson and Enabled play opposing roles downstream of the roundabout receptor. Cell 101, 703–715. [PubMed: 10892742]
60. DeGeer J, Boudeau J, Schmidt S, Bedford F, Lamarche-Vane N, and Debant A (2013). Tyrosine phosphorylation of the Rho guanine nucleotide exchange factor Trio regulates netrin-1/DCC-mediated cortical axon outgrowth. Mol. Cell Biol 33, 739–751. 10.1128/MCB.01264-12. [PubMed: 23230270]
61. Demarco RS, Struckhoff EC, and Lundquist EA (2012). The Rac GTP exchange factor TIAM-1 acts with CDC-42 and the guidance receptor UNC-40/DCC in neuronal protrusion and axon guidance. PLoS Genet. 8, e1002665. 10.1371/journal.pgen.1002665. [PubMed: 22570618]
62. Hu H, Li M, Labrador JP, McEwen J, Lai EC, Goodman CS, and Bashaw GJ (2005). Cross GTPase-activating protein (CrossGAP)/Vilse links the Roundabout receptor to Rac to regulate midline repulsion. Proc. Natl. Acad. Sci. USA 102, 4613–4618. [PubMed: 15755809]
63. Yang L, and Bashaw GJ (2006). Son of sevenless directly links the Robo receptor to rac activation to control axon repulsion at the midline. Neuron 52, 595–607. 10.1016/j.neuron.2006.09.039. [PubMed: 17114045]
64. Lundström A, Gallio M, Englund C, Steneberg P, Hemphälä J, Aspenström P, Keleman K, Falileeva L, Dickson BJ, and Samakovlis C (2004). Vilse, a conserved Rac/Cdc42 GAP mediating Robo repulsion in tracheal cells and axons. Genes Dev. 18, 2161–2171. [PubMed: 15342493]
65. O'Donnell MP, and Bashaw GJ (2013). Distinct functional domains of the Abelson tyrosine kinase control axon guidance responses to Netrin and Slit to regulate the assembly of neural circuits. Development 140, 2724–2733. 10.1242/dev.093831. [PubMed: 23720041]
66. Hsouna A, Kim YS, and VanBerkum MFA (2003). Abelson tyrosine kinase is required to transduce midline repulsive cues. J. Neurobiol 57, 15–30. [PubMed: 12973825]
67. Lebrand C, Dent EW, Strasser GA, Lanier LM, Krause M, Svitkina TM, Borisy GG, and Gertler FB (2004). Critical role of Ena/VASP proteins for filopodia formation in neurons and in function downstream of netrin-1. Neuron 42, 37–49. 10.1016/S0896-6273(04)00108-4. [PubMed: 15066263]
68. Wills Z, Emerson M, Rusch J, Bikoff J, Baum B, Perrimon N, and Van Vactor D (2002). A Drosophila homolog of cyclase-associated proteins collaborates with the Abl tyrosine kinase to control midline axon pathfinding. Neuron 36, 611–622. [PubMed: 12441051]
69. Bashaw GJ, and Klein R (2010). Signaling from axon guidance receptors. Cold Spring Harbor Perspect. Biol 2, a001941. 10.1101/cshperspect.a001941.
70. Shoja-Taheri F, DeMarco A, and Mastick GS (2015). Netrin1-DCC-Mediated attraction guides post-crossing commissural axons in the hindbrain. J. Neurosci 35, 11707–11718. 10.1523/JNEUROSCI.0613-15.2015. [PubMed: 26290247]
71. Bonanomi D, Valenza F, Chivatakarn O, Sternfeld MJ, Driscoll SP, Aslanian A, Lettieri K, Gullo M, Badaloni A, Lewcock JW, et al. (2019). p190RhoGAP filters competing signals to Resolve axon guidance conflicts. Neuron 102, 602–620.e9. 10.1016/j.neuron.2019.02.034. [PubMed: 30902550]
72. Bai G, Chivatakarn O, Bonanomi D, Lettieri K, Franco L, Xia C, Stein E, Ma L, Lewcock JW, and Pfaff SL (2011). Presenilin-dependent receptor processing is required for axon guidance. Cell 144, 106–118. 10.1016/j.cell.2010.11.053. [PubMed: 21215373]
73. Delloye-Bourgeois C, Jacquier A, Charoy C, Reynaud F, Nawabi H, Thoinet K, Kindbeiter K, Yoshida Y, Zagar Y, Kong Y, et al. (2015). PlexinA1 is a new Slit receptor and mediates axon guidance function of Slit C-terminal fragments. Nat. Neurosci 18, 36–45. [PubMed: 25485759]

74. Cong L, Ran FA, Cox D, Lin S, Barretto R, Habib N, Hsu PD, Wu X, Jiang W, Marraffini LA, and Zhang F (2013). Multiplex genome engineering using CRISPR/Cas systems. Science 339, 819–823. 10.1126/science.1231143. [PubMed: 23287718]

75. Matsuda T, and Cepko CL (2004). Electroporation and RNA interference in the rodent retina in vivo and in vitro. Proc. Natl. Acad. Sci. USA 101, 16–22. 10.1073/pnas.2235688100. [PubMed: 14603031]

76. Junge HJ, Yung AR, Goodrich LV, and Chen Z (2016). Netrin1/DCC signaling promotes neuronal migration in the dorsal spinal cord. Neural Dev. 11, 19. 10.1186/s13064-016-0074-x. [PubMed: 27784329]

Highlights

- Two DCC receptor isoforms are required to achieve proper Netrin1 signaling *in vivo*
- DCC_L and DCC_S adopt different conformations and have distinct signaling abilities
- Solely expressing DCC_L or DCC_S alters axon growth, attraction, and fasciculation
- Netrin1/DCC_L together with ROBO3.1 antagonizes Slit/ROBO1 signaling

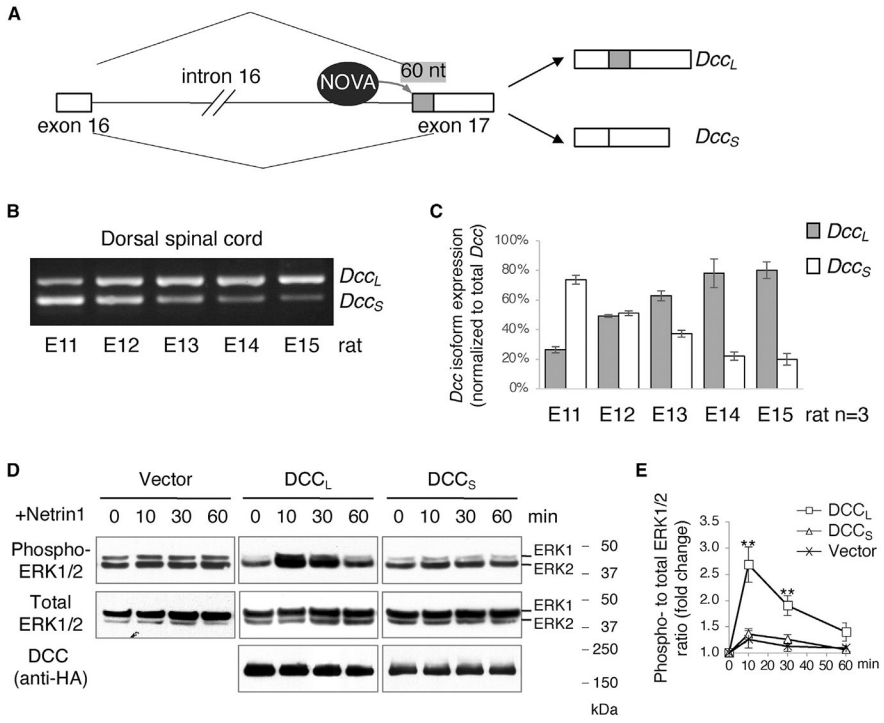

Figure 1. Two distinct *Dcc* isoforms are expressed during commissural axon guidance

(A) Alternative splicing between exons 16 and 17 generates two *Dcc* isoforms that differ in 60 nt (shaded in gray). NOVA family of splicing factors bind *Dcc* pre-mRNA and promote Dcc_L production.

(B and C) *Dcc* isoform expression measured by semi-quantitative and quantitative RT-PCR, respectively. Both isoforms are expressed during commissural neurogenesis and axon guidance (E11–E15 in rats, equivalent to E9.5 to E13.5 in mice. Rat embryos were used to facilitate microdissection of the DSC). Data in (C) were collected from three embryos and are presented as mean ± SD.

(D and E) DCC isoforms have distinct abilities to stimulate ERK1/2 phosphorylation upon Netrin1 stimulation (250 ng/mL for the indicated durations). (E) Quantification of ERK1/2 phosphorylation in (D). Data were collected from three independent experiments and are presented as mean ± SD. Two-way ANOVA was performed with a Tukey post hoc test (**$p < 0.01$).

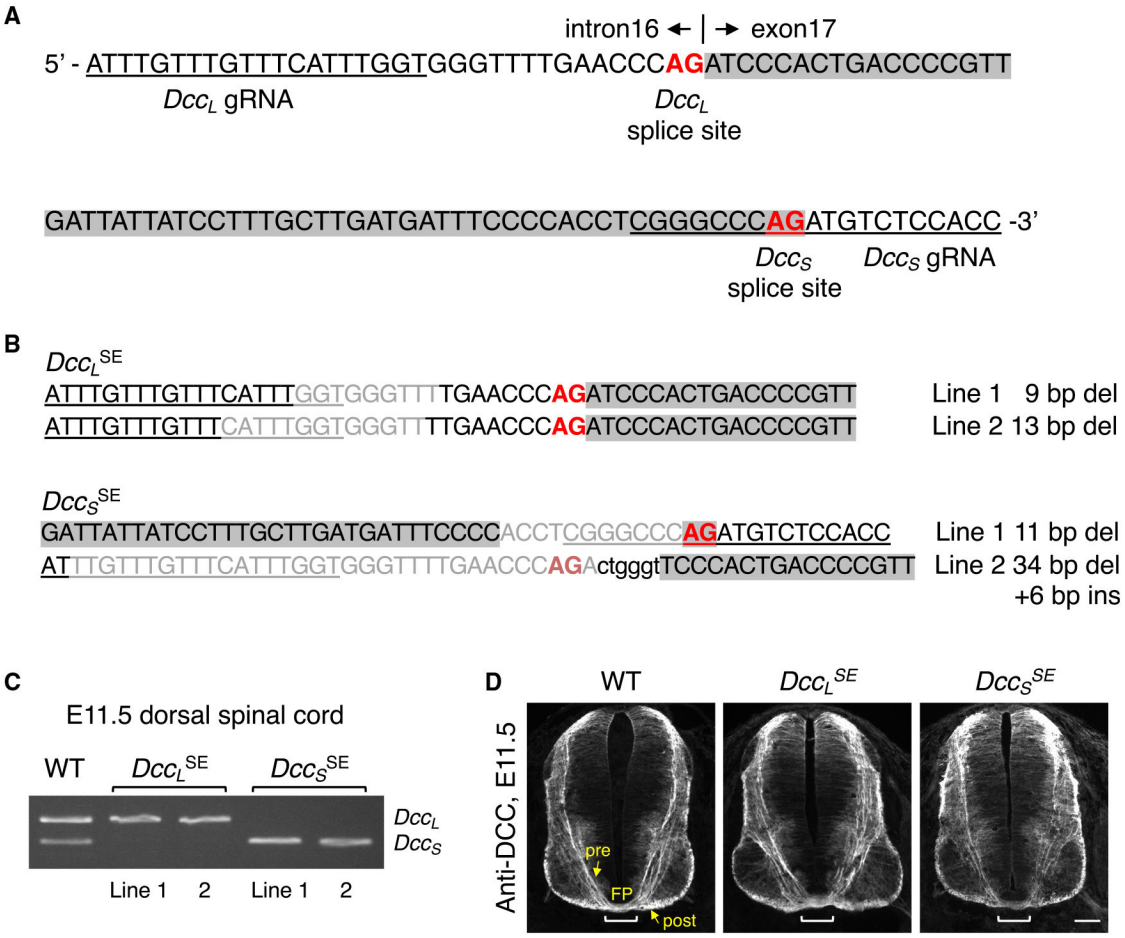

Figure 2. Generation of CRISPR-Cas9-engineered mouse models for *Dcc* isoforms

(A) Design of guide RNAs (gRNAs) for *Dcc* isoforms. Targeted nucleotides of the gRNAs are underlined, and the alternative splice sites are in red.

(B) Genomic mutations in two independent founder lines for each *Dcc* isoform. Deleted nucleotides are in lighter gray and inserted nucleotides in lower case.

(C) Only one isoform is produced in *Dcc* isoform mutants, measured by semi-quantitative RT-PCR. Both isoforms are expressed in wild-type (WT) controls at E11.5.

(D) Anti-DCC staining of transverse spinal cord sections from WT and *Dcc* isoform mutant embryos at E11.5. DCC is present in both pre- and post-crossing axonal segments (yellow arrows). Brackets indicate the floorplate (FP) area. *Dcc* is also expressed in ipsilateral-projecting interneurons and motor neurons.[37] Scale bar, 100 μm.

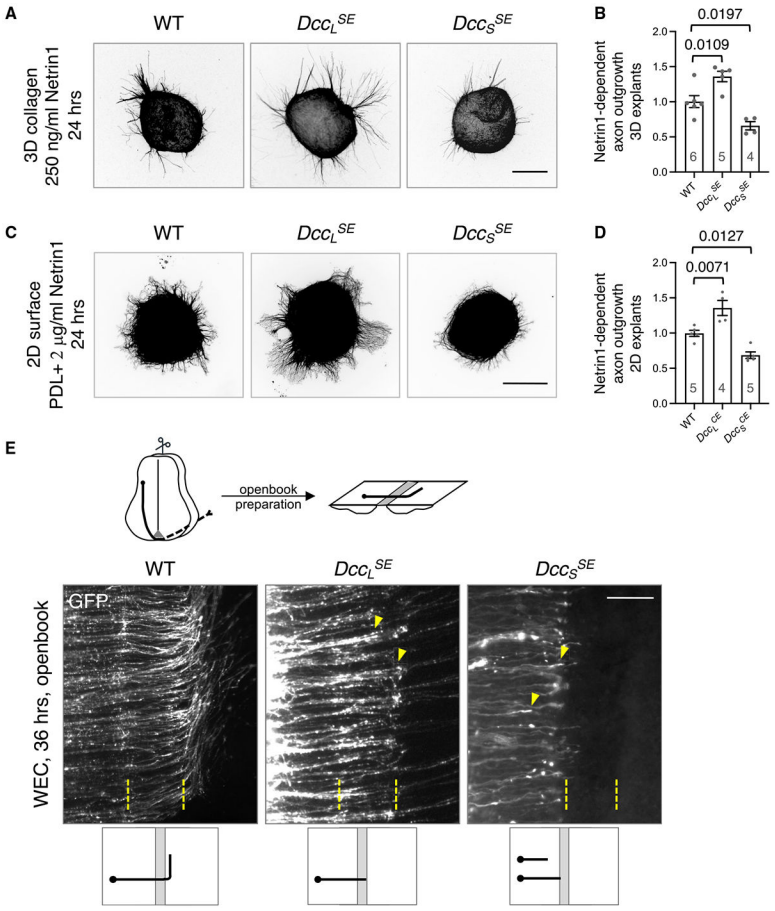

Figure 3. Expressing only one of two DCC isoforms differentially affects commissural axon outgrowth and guidance

(A and C) Axon outgrowth from dorsal spinal cord (DSC) explants in response to bath-applied Netrin1 in 3D collagen matrix (A) and to Netrin1 coated on 2D surface (C), respectively (Netrin1 concentration and culture period as indicated). Under both conditions, axon outgrowth was increased in Dcc_L^{SE} mutants but was reduced in Dcc_S^{SE} mutants.

(B and D) Quantification of axon outgrowth in (A) and (C), respectively; 3–5 explants were examined for each embryo. Data were normalized to WT controls and are presented as mean ± SD. One-way ANOVA with a Dunnett post hoc test; p values and animal numbers as indicated.

(E) Axon projection around the midline in cultured whole embryos. The spinal cord was cut open at the dorsal midline and flattened in an open-book configuration to allow visualization of the FP area. A *Gfp* reporter was electroporated unilaterally into the DSC. Within 36 h of culturing (E10 to the equivalent of E11.5), WT axons were able to enter and exit the FP and make a sharp turn on the contralateral side (dashed lines indicate the FP boundaries). Dcc_L^{SE} axons entered the FP normally, but the majority stalled within or at the contralateral boundary of the FP (two examples are highlighted with arrowheads). By contrast, most Dcc_S^{SE} axons had not reached or entered the FP by the end of culturing (examples highlighted by arrowheads). Scale bars, 100 μm.

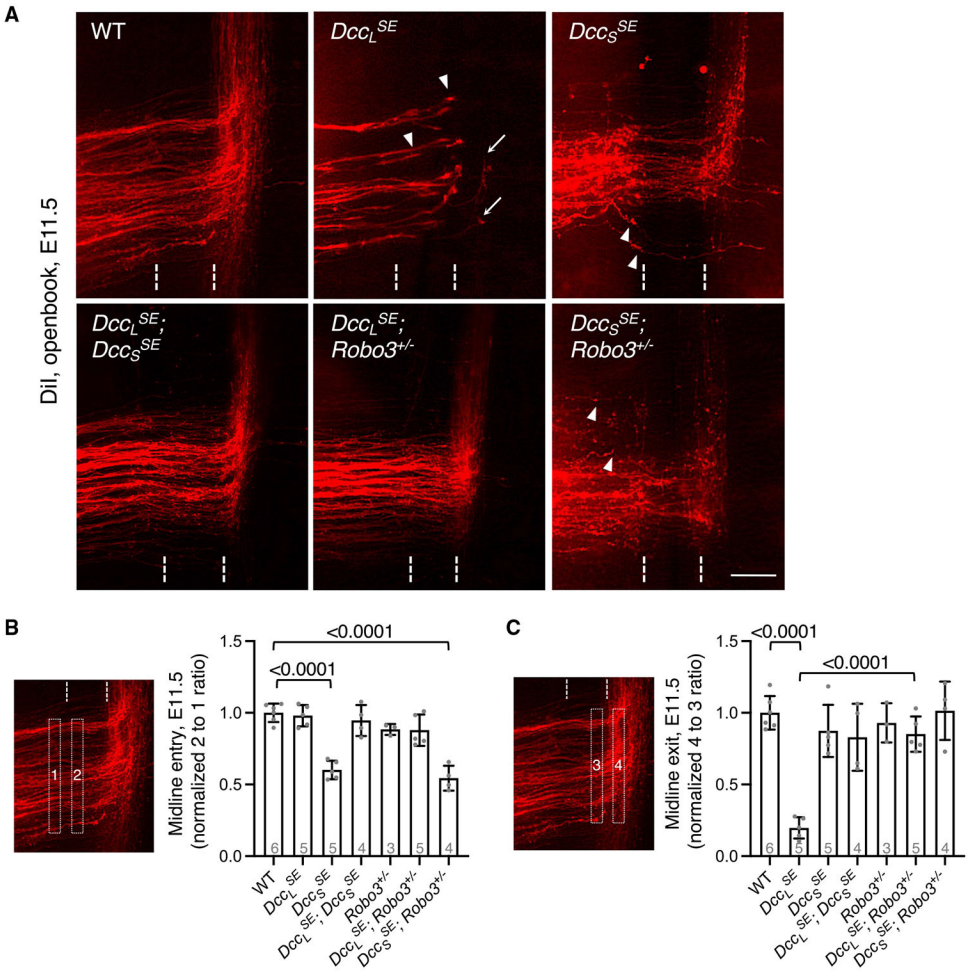

Figure 4. Expressing only one of two DCC isoforms differentially disrupts midline entry and exit

(A) DiI tracing of spinal commissural axons from WT controls and different mutants in an open-book orientation. At E11.5, WT axons had projected across the FP and made a sharp turn upon exit. Most Dcc_L^{SE} axons stalled within the FP, and the axons were present in bundles (arrowheads). Only a small number of axons had exited the FP and were present as single axons (arrows). Many Dcc_S^{SE} axons stalled before entering the FP at E11.5 (arrowheads). In Dcc_L^{SE}; Dcc_S^{SE} transheterozygotes, the axons entered and exited the midline normally. A heterozygous *Robo3* KO allele facilitated midline exit when it was introduced into Dcc_L^{SE} mutants. $Robo3^{+/-}$ by itself does not cause significant guidance defects.[7,18,43] Scale bar, 100 μm.

(B and C) Quantification of midline entry (B) and exit (C), respectively, by DiI tracing at E11.5. The signals from four boxed areas were measured with ImageJ. The ratio between areas 2 and 1 represents midline entry, and the ratio between areas 4 and 3 represents midline exit. Data were normalized to WT controls and are presented as mean ± SD. One-way ANOVA with a Tukey post hoc test; p values and animal numbers as indicated.

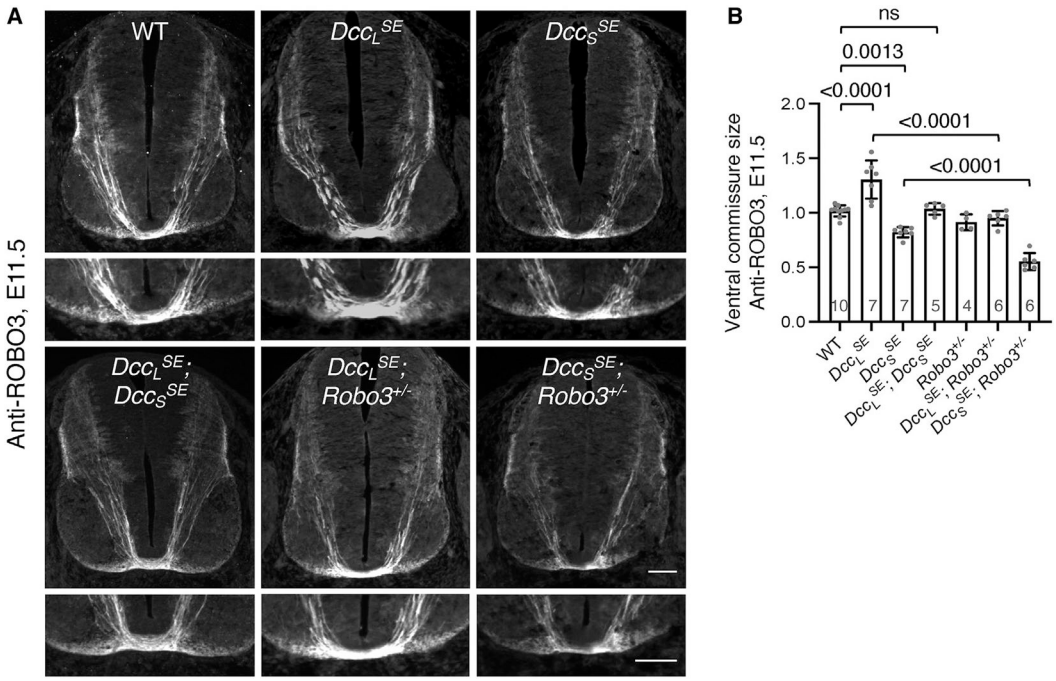

Figure 5. Expressing only one of two DCC isoforms differentially affects the ventral commissure size

(A) Ventral projection and midline crossing of commissural axons examined by anti-ROBO3 staining of transverse spinal cord sections at E11.5. Bottom panels show close-up of the FP. The ventral commissure was thicker in Dcc_L^{SE} mutants but was thinner in Dcc_S^{SE} mutants at E11.5. Transheterozygous Dcc_L^{SE}; Dcc_S^{SE} mutants had normal-sized ventral commissure. Reducing *Robo3* dose decreased the commissure size in both *Dcc* isoform mutants. Scale bars, 100 μm.

(B) Quantification of ventral commissure size by anti-ROBO3 staining. The commissure size is quantified as the ratio between the thickness of the ventral commissure and the height of the FP. Data were normalized to WT controls and are presented as mean ± SD. One-way ANOVA with a Tukey post hoc test; p values and animal numbers as indicated; ns, not significant.

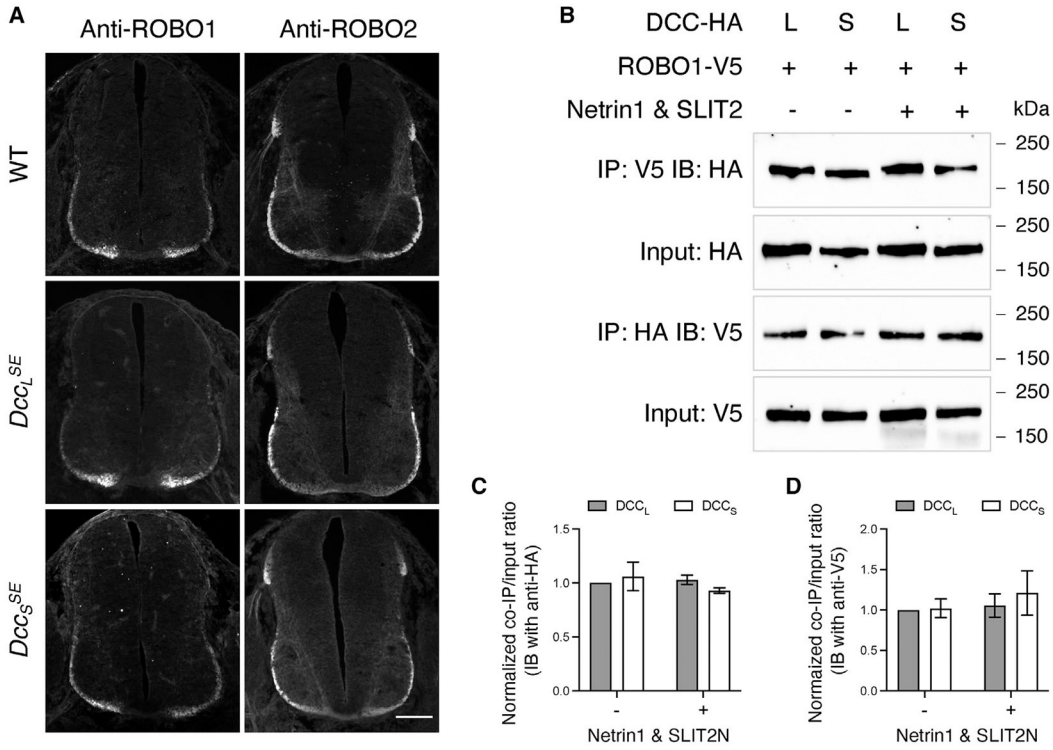

Figure 6. ROBO1 localization is unaffected in *Dcc* isoform mutants and ROBO1 binds both DCC isoforms

(A) Anti-ROBO1 and anti-ROBO2 staining of transverse spinal cord sections at E11.5. In both WT and *Dcc* isoform mutants, ROBO1 and ROBO2 are present at low levels in pre-crossing axonal domains but become highly upregulated post crossing. *Robo1/2* are also expressed in ipsilateral-projecting interneurons and motor neurons.[18] Scale bar, 100 μm.

(B) CoIP between DCC isoforms and ROBO1. Hemagglutinin (HA)-tagged DCC (L, long; S, short) and V5-tagged ROBO1 were coexpressed in COS-1 cells in the absence or presence of Netrin1 and SLIT2N stimulation (250 ng/mL each for 30 min).

(C and D) Quantification of DCC and ROBO1 interaction from immunoblotting (IB) with anti-HA (C) and anti-V5 (D). Data were collected from three independent experiments and are presented as mean ± SD. Two-way ANOVA was performed with a Tukey post hoc test (not significant for all data points). Both DCC isoforms interacted with ROBO1 and at comparable levels, with or without ligand stimulation.

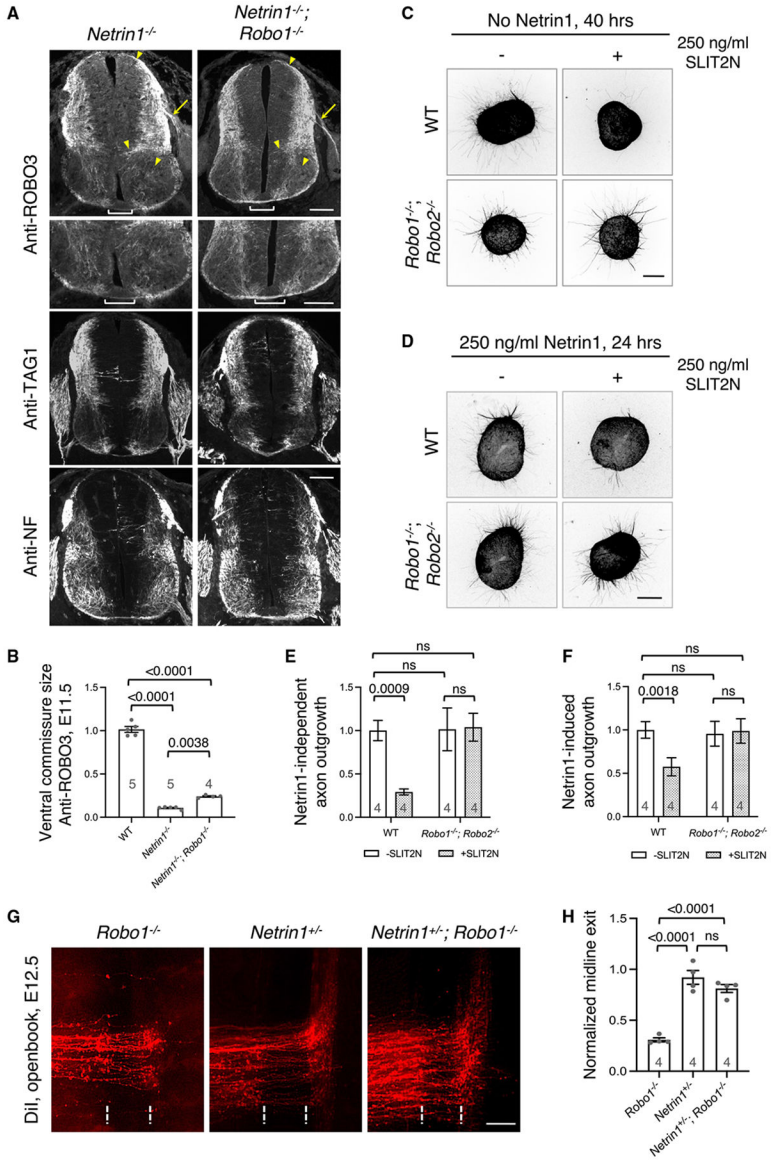

Figure 7. Netrin1/DCC and SLIT/ROBO1 signaling antagonize each other during midline entry and exit

(A) Axon projection and midline crossing in compound *Netrin1* and *Robo1* KO mutants, examined by anti-ROBO3, anti-TAG1, and anti-NF staining of transverse spinal cord sections at E11.5. *Netrin1*$^{-/-}$ null mutants exhibited severe guidance defects in the spinal cord, including misprojections into the roof plate, ventricular zone, and motor columns (highlighted with yellow arrowheads), abnormal exit from the CNS (yellow arrow), and an almost complete absence of the ventral commissure (bracket). Removing *Robo1* allowed more axons to cross the midline in *Netrin1*$^{-/-}$ null background (the ventral commissure indicated by the bracket is thicker in *Netrin1*$^{-/-}$*; Robo1*$^{-/-}$ embryos), but other guidance errors, indicated by yellow arrowheads and yellow arrows, persisted.

(B) Quantification of the ventral commissure size in (A). Anti-ROBO3 was used as it does not label any motor axons.[38]

(C and D) Effect of bath-applied SLIT2N (250 ng/mL) on DSC axon outgrowth in the absence and presence of Netrin1, respectively. Explants were cultured in 3D collagen matrix for 40 h without Netrin1 in (C) and for 24 h with 250 ng/mL bath-applied Netrin1 in (D). SLIT2N repressed WT axon outgrowth regardless of whether Netrin1 was present but did not inhibit the growth from *Robo1/2* double KO explants.

(E and F) Quantification of axon outgrowth in (C) and (D), respectively.

(G) DiI tracing of spinal commissural axons in an open-book orientation in compound *Netrin1* and *Robo1* KO mutants. Most *Robo1*$^{-/-}$ axons stalled within and at the contralateral boundary of the FP at E12.5. Introduction of a heterozygous *Netrin1* KO allele into *Robo1*$^{-/-}$ mutant background allowed more axons to exit. Scale bars, 100 μm.

(H) Quantification of midline exit in (G). See Figure 4C for description of quantification. Data were normalized to WT controls and are presented as mean ± SD. One-way ANOVA with a Tukey post hoc test in (B) and (H), two-way ANOVA with a Tukey post hoc test in (E) and (F); p values and animal numbers as indicated; ns, not significant; 5–10 sections, 3–5 explants, and 3–5 DiI injection sites were quantified for each embryo.

KEY RESOURCES TABLE

REAGENT or RESOURCE	SOURCE	IDENTIFIER
Antibodies		
Mouse anti-DCCin (intracellular domain)	Novus Biologicals	MAB5884, Clone 531505
Goat-anti-DCCecto (extracellular domain)	R&D	AF844
Goat-anti-TAG1	R&D	AF4439
Mouse-anti-NF	Developmental Studies Hybridoma Bank	2H3
Goat-anti-ROBO1	R&D	AF1749
Rabbit anti-ROBO2	Cell Signaling Technology	E4M6D
Rabbit anti-ROBO3	Chen et al.[26]	N/A
Rabbit anti-ROBO3.1	Chen et al.[26]	N/A
Rabbit anti-phosphoERK1/2 (Thr202/Tyr204)	Cell Signaling Technology	9101
Rabbit anti-ERK1/2	Cell Signaling Technology	9102
Rabbit anti-V5 resin	Abcam	ab1229
Anti-V5-HRP	ThermoFisher Scientific	R96125
Rat anti-HA resin	Roche	11815016001
Rat anti-HA-HRP	Roche	12013819001
Rabbit anti-β-TubulinIII	Sigma-Aldrich	T3952
Goat-anti-Rabbit-HRP	Jackson ImmunoResearch	111-035-144
Donkey anti-goat Alexa Fluor594	Jackson ImmunoResearch	705-585-147
Donkey anti-rabbit Alexa Fluor594	Jackson ImmunoResearch	711-585-152
Donkey anti-mouse Alexa Fluor594	Jackson ImmunoResearch	715-585-150
Mouse anti-βActin-HRP	Sigma	A3854
Rat anti-mouse TrueBlot Ultra-HRP	Rockland	18-8817-30
Chemicals, peptides, and recombinant proteins		
Netrin1	R&D	1109-N1
SLIT2 N-term (SLIT2N)	BioLegend	757104
Critical commercial assays		
MEGAscript T7 Transcription Kit	ThermoFisher Scientific	AMB13345
MEGAclear transcription cleanup kit	ThermoFisher Scientific	AM1908
Experimental models: Cell lines		
COS-1	ATCC	CRL-1650
Experimental models: Organisms/strains		
Mouse: CD-1	Charles River Laboratories	Crl:CD1(ICR)
Mouse: FVB (for pronuclear injection)	The Jackson Laboratory	Strain #:001800 RRID:IMSR_JAX:001800
Mouse: *Netrin1* knockout	Yung et al.[47]	N/A
Mouse: *Robo1* knockout	Long et al.[24]	N/A
Mouse: *Robo1; Robo2* knockout	Chen et al.[26]	N/A
Mouse: *Robo3* knockout	Sabatier et al.[18]	N/A
Rat: Sprague Dawley rats	Charles River Laboratories	Crl:SD

REAGENT or RESOURCE	SOURCE	IDENTIFIER
Oligonucleotides		
Guide RNA for DCC_L: ATTTGTTTGTTTCATTTGGTggg (PAM sequence in lower case)	This paper	N/A
Guide RNA for DCC_S: GGTGGAGACATCTGGGCCCGagg (PAM sequence in lower case)	This paper	N/A
Genotyping primers for DCC isoforms mutants	This paper (see Table S1)	N/A
Primers for quantitative and semi-quantitative RT-PCR	This paper (see Table S2)	N/A
Recombinant DNA		
pX330 (humanized coding sequence of *S. pyogenes* CAS9	Cong et al.[74]	Addgene 42230
spCas9 in pJET1.2	This paper	N/A
Dcc alternative splicing reporter	Leggere et al.[33]	N/A
pCR2.1TOPO	ThermoFisher Scientific	K450002
pCAS-GFP	Matsuda and Cepko[75]	Addgene 11150
DCC_L-HA	Leggere et al.[33]	N/A
DCC_S-HA	Leggere et al.[33]	N/A
ROBO1(e6b+)-V5	This paper	N/A
Software and algorithms		
Fiji	NIH	https://fiji.sc/
GraphPad Prism 9	GraphPad	https://www.graphpad.com/